Marine Structures 23 (2010) 22–38

Contents lists available at ScienceDirect

Marine Structures

journal homepage: www.elsevier.com/locate/marstruc

Hydro-elastic analysis and optimization of a composite marine propeller

José Pedro Blasques*, Christian Berggreen, Poul Andersen

Department of Mechanical Engineering, Technical University of Denmark, Nils Koppels Allé, Building 403, DK 2800 Kgs. Lyngby, Denmark

ARTICLE INFO

Article history:
Received 19 December 2008
Received in revised form
18 September 2009
Accepted 19 October 2009

Keywords:
Marine propellers
Composite
Hydro-elastic
Optimization
Strength analysis

ABSTRACT

The present paper addresses the design and optimization of a flexible composite marine propeller. The aim is to tailor the laminate to control the deformed shape of the blade and consequently the developed thrust. The development of a hydro-elastic model is presented, and the laminate lay-up which minimizes the fuel consumption for the cruising and maximum speed conditions is simultaneously determined. Results show a reduction of 1.25% in fuel consumption for the combined case corresponding to a decrease of 4.7% in the cruising speed condition. Finally, the strength of the optimal blade is analyzed using the Tsai-Wu strength index. After local tailoring of the laminate configuration throughout the propeller a maximum value of 0.7 is determined indicating no failure will occur under normal operation conditions. The results suggest that it is possible to design a medium-sized flexible composite marine propeller that will enable a reduction of the fuel consumption while withstanding the imposed loads

1. Introduction

Anisotropic composite materials present different levels of elastic couplings which depend on the laminate lay-up. Among these, bending- and extension-twist couplings have been identified as a possible mean for the passive control of composite structures. The aim here is to investigate the possibility of tailoring these elastic couplings to control the performance of a flexible composite

* Corresponding author. Tel.:+45 4525 1379; fax: +45 45884325.
E-mail address: jpb@mek.dtu.dk (J.P. Blasques).

0951-8339/$ – see front matter © 2009 Elsevier Ltd. All rights reserved.
doi:10.1016/j.marstruc.2009.10.002

marine propeller. The shape of the propeller blade will morph under load and thus, if optimized, it will passively adjust itself to the hydrodynamic loads of the different operational conditions. The optimal composite propeller is the one which minimizes the fuel consumption.

The use of elastic couplings to control the passive properties of different structures like wind turbine blades [1,2,3], aircraft wings [4] and helicopter rotor blades [5] has been extensively reported in the literature. The literature concerning the application of laminated composite materials in the design of marine propellers is however limited. Lee et al. [6] have optimized the laminate lay-up of a fixed pitch 0.305 m diameter composite marine propeller using genetic algorithms. The final composite design presents lower values of torque at one of the operation conditions thus outperforming its metal counterpart. An evaluation of the strength properties of a composite propeller blade with 1.4 m diameter has been presented by Lin et al. [7]. The strength is analysed using the Hashin failure criterion and the results illustrate the influence of the laminate type on the stress field and failure modes. Marsh [8] has presented an overview of the developments in the composite propeller industry. A few companies have realized the potential and claim to have designed composite marine propellers with passive properties. Nonetheless, no details of these developments have yet been published.

The work described in this paper extends the available knowledge in the field of design and optimization of composite marine propellers, with special focus on medium size marine propellers. The propeller blade considered throughout this paper is approximately four times larger than those described earlier in the literature. The results presented in this paper will indicate if the possibility and potential of using composite propeller blades in large merchant or naval vessels exists. The hydrodynamic model is based on the boundary element method instead of the lifting line method applied in earlier papers. Moreover, the optimization of the fiber orientations is combined with the strength analysis in one design process. The two analyses have earlier been treated separately.

2. Blade geometry and material properties

The original propeller blade is part of a controllable pitch propeller installed in a naval vessel. The propeller has 4 blades, a diameter, D, of 4.4 m and an expanded area ratio of 0.56. The main geometrical properties of the blade are presented in Table 1 where R is the propeller radius, r is the section radius, θ_{skew} is the sectional skew angle, *Rake* is the sectional rake, P is the sectional pitch, c is the section cord, t is the maximum section thickness and f is the section camber.

Naval vessels typically operate at two very distinct forward speed conditions – herein named cruising and maximum speed conditions – as presented in Table 2. The non-dimensional thrust and torque coefficients K_T and K_Q are defined as

$$K_T = \frac{T}{\rho n^2 D^4}, \quad K_Q = \frac{Q}{\rho n^2 D^5} \tag{1}$$

where T, Q, ρ and n are the thrust, torque, sea water density and rotational speed, respectively. The service speed, advance ratio, non-dimensional pitch at $r/R = 0.7$, the open water efficiency and the fuel consumption are identified as V_s, J, P/D_{07}, η_0 and FC, respectively.

Table 1
Geometrical properties of the propeller blade.

r/R	θ_{skew} [o]	Rake/R	P/D	c/D	t/c	f/c
0.300	0.000	0.0000	0.90665	0.200	0.195	0.000
0.350	−6.033	0.0006	1.02277	0.230	0.159	0.032
0.400	−10.156	−0.0018	1.13893	0.260	0.131	0.040
0.500	−16.663	−0.0250	1.30864	0.320	0.091	0.036
0.600	−16.663	−0.0309	1.42662	0.360	0.067	0.027
0.700	−6.033	−0.0787	1.46216	0.385	0.050	0.020
0.800	6.542	−0.0910	1.38514	0.380	0.037	0.015
0.900	20.141	−0.0807	1.1867	0.320	0.029	0.009
1.000	36.932	−0.0299	0.8685	0.050	0.086	0.000

Table 2
Characterization of the cruising and maximum speed operation conditions. Thrust and torque coefficients are for one blade only.

	Power [kW]	n [rps]	V_s [m/s]	J [−]	P/D_{07} [−]	K_T [−]	K_Q [−]	η_0 [−]	FC [kg/h]
Cruising Speed	1410	1.8	7	0.742	0.925	0.056	0.0091	0.59	26.83
Max. Speed	8380	2.33	11	0.901	1.465	0.176	0.0363	0.65	662.1

The composite marine propeller was designed using carbon/epoxy uni-directional reinforcements with mechanical properties presented in Table 3 (from [9]).

The laminate lay-up will be described using the notation $[(\theta_i)_j]_s$ where the subscript i indicates the design variable numbering and j refers to the number of layers oriented with the angle θ. The layers are assumed to be stacked from pressure side to suction side. Finally, the subscript s indicates symmetry with respect to the mid-thickness plane.

3. Methodology

The initial step in the analysis of the composite propeller consists of the development of the structural and hydrodynamic models. The two models are then combined into a hydro-elastic model which, for a steady incoming flow, determines the equilibrium between the structural and hydrodynamic forces. An optimization algorithm is used next to determine the laminate lay-up which will minimize the fuel consumption. Finally, the strength of the optimal blade is analyzed.

3.1. Structural model

The structural model is able to determine the deformation and stress fields induced by a given hydrodynamic pressure load on the blade. The model is generated and analyzed in the commercial finite element package ANSYS 11 [10]. The blade geometry is approximated by a surface defined by the mid-thickness lines of each section. The surface is subsequently meshed with 8 node isoparametric parabolic layered shell elements (SHELL99). The element thickness or the total laminate thickness at a given node is obtained by linear interpolation of the thickness of the blade at the corresponding position (see Fig. 1(a)). The layer fiber angles are controlled at each element independently.

The displacement degrees of freedom of all nodes at the blade root are constrained to simulate the attachment to the propeller hub. The centrifugal forces are applied as accelerations which are function of the rotational speed. The number of layers is assumed constant and fixed throughout the whole

Table 3
Mechanical properties of the High Tension Carbon/Epoxy uni-directional reinforcement. Subscripts x, y and z refer to the fiber, matrix and out-of-plane directions, respectively. The subscript t and c indicate tension and compression failure, respectively.

	Symbol	Units	
Stiffness Modulus	E_x	GPa	135
	E_y	GPa	15
	E_z	GPa	15
Shear Modulus	G_{xy}	GPa	5
	G_{xz}	GPa	5.3
	G_{yz}	GPa	2.9
Poisson's Ratio	ν_{xy}	–	0.3
	ν_{xz}	–	0.02
	ν_{yz}	–	0.02
Ult. Tensile Strength	$\sigma^f_{x_t}$	MPa	1500
	$\sigma^f_{y_t}$	MPa	50
Ult. Comp. Strength	$\sigma^f_{x_c}$	MPa	1200
	$\sigma^f_{y_c}$	MPa	250
Ult. Shear Strength	σ^f_{xy}	MPa	70
Density	ρ^f	kg/m^3	1600
Thickness	t	mm	0.3

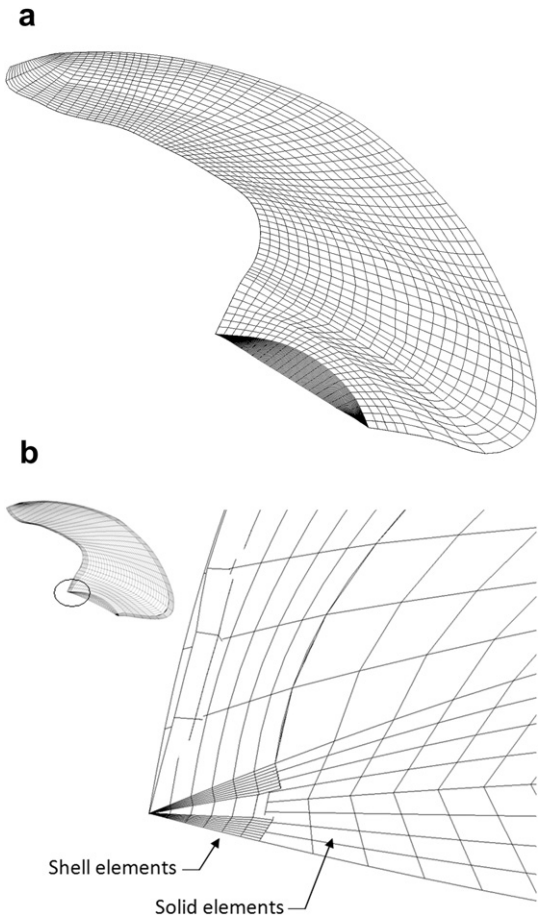

Fig. 1. (a) Aspect of the shell element model seen from the hub towards the tip. The thickness of the elements has been made visible through a graphical artifice in ANSYS. It is possible to observe the thickness variation throughout the elements and thus the shape of the blade. (b) Detail of the solid element model in the trailing edge region seen from the hub towards the tip. The layered solid elements with a total of 8 layers (2 rows of solid elements through the thickness with 8 layers each) are visible together with the shell elements with varying thickness used to mesh the trailing edge.

blade. Furthermore, all layers are assumed to have the same thickness which is a fixed portion of the total blade thickness at the corresponding point of the blade. A mesh convergence analysis aimed at displacements and stresses is conducted. The static analyses showed that a total of 1440 and 5760 shell elements are required for the convergence of the displacement and stress fields, respectively (see Fig. 2(a) and (b)). This model is henceforth named *shell element model*.

Since experimental data are not available to validate the results from the shell element model, a second numerical model is developed as well. In this second model – addressed as *solid element model* – the shape of the blade is defined by its volume. The center part of the blade excluding the leading and trailing edges are meshed using 20 node isoparametric parabolic layered solid elements (SOLID191), whereas the leading and trailing edges (covering approximately 1/16 of the chord length) are meshed with shell elements (SHELL99) (see Fig. 1(b)). An additional layer of shell elements with low stiffness is applied on the solid elements adjacent to the leading and trailing edge. By adopting this approach it is possible to ensure that the deformations contained in the rotational degrees of freedom of the shell elements are partially transferred to the solid elements containing only translational degrees of freedom. The boundary conditions are the same as used before for the shell element model.

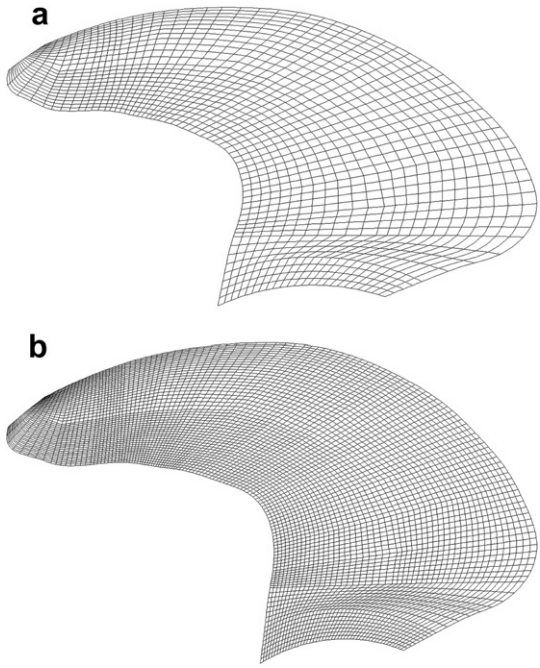

Fig. 2. Shell model mesh: (a) Mesh applied in displacement analysis. (b) Mesh applied in stress analysis. Special care has been devoted to the mesh at the tip region where the elements can suffer large distortions.

The static analyses in this case have shown that a total of 4400 elements are required for both displacement and stress convergence.

The two models are subsequently compared in terms of their ability to predict the influence of the laminate lay-up on the thrust and torque forces. The results are presented in Fig. 3 where it is assumed that the entire blade consists of the same lay-up, $[(\theta)_{32}]$, and hence all layers have the same orientation angle θ. The thrust and torque coefficients are then analyzed as a function of the angle variation, θ. By comparing the two models, it can be seen that the results are in good agreement with a maximum relative difference of 1.4%, implying that the displacement fields predicted by the two models are identical.

All results presented hereafter are obtained using the shell element model. This model is chosen because it requires a shorter computational time which is a critical aspect for the optimization procedure.

3.2. Hydrodynamic model

The hydrodynamic model is used to determine the pressure field induced by a given blade shape. It is based on the boundary element method and assumes that the inflow to the propeller is uniform and steady. Viscous forces have been neglected. A total of 480 section points define the 450 elements which are arranged in a 15×15 three-dimensional structured mesh on both faces of the blade (see Fig. 4).

The pressure is then determined at 450 nodes placed at the center of each element whose corners are defined by the section points (which define the section lines). The pressure distribution is illustrated in Fig. 5. The pressure is furthermore integrated over the hydrodynamic model mesh to determine the values of thrust and torque.

3.3. Hydro-elastic model

The displacement field, {d}, is determined using the finite element method in the structural model, and the hydrodynamic pressure field, {f}, is determined using the boundary element method in the

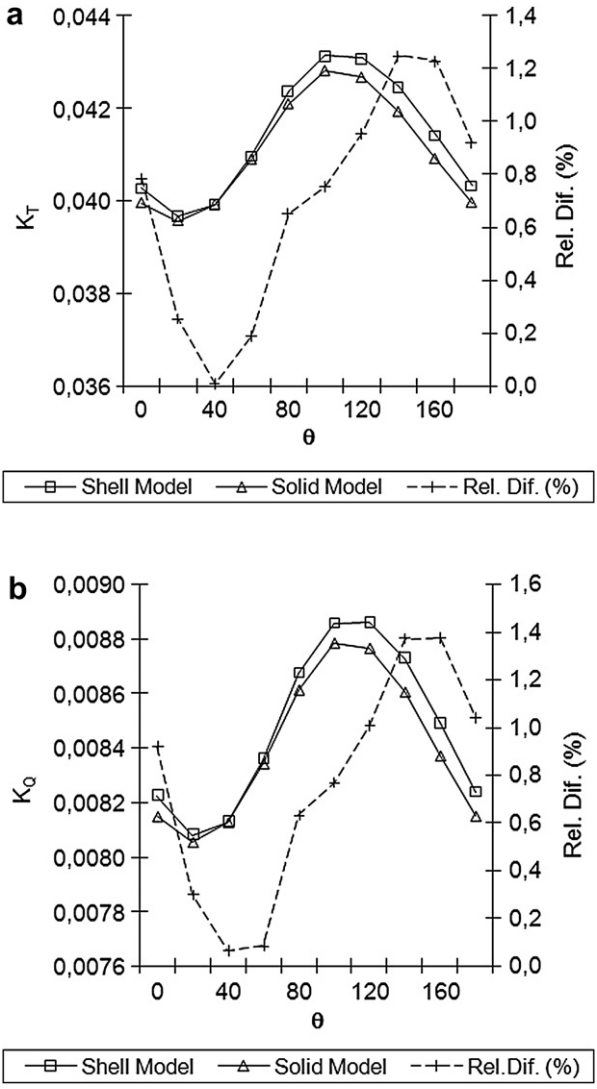

Fig. 3. Thrust (a) and torque (b) coefficients – K_T and K_Q, respectively – and relative difference as a function of the laminate angle θ for the shell and solid element models. The entire blade consists of the same uni-angle laminate lay-up. Results are for one blade only.

hydrodynamic model. The equilibrium between the hydrodynamic and structural forces is obtained by the hydro-elastic model. That is, the hydro-elastic model determines the displacement vector {d} which satisfies $[K]\{d\} = \{f\}$, where K is the structural stiffness matrix which can be tailored by optimizing the laminate lay-up sequence. Since {f} is a function of {d} the problem is nonlinear. However, {f} is only dependent on {d} which makes the problem suited for an iterative solution. The direct substitution method has been chosen.

A schematic description of the algorithm is presented in Fig. 6 where the subscript i indicates the iteration number. Each of the numbered steps is described below:

1) The displacement field is determined by the structural model for a given pressure distribution. At the first iteration the pressure distribution is that of the original blade.

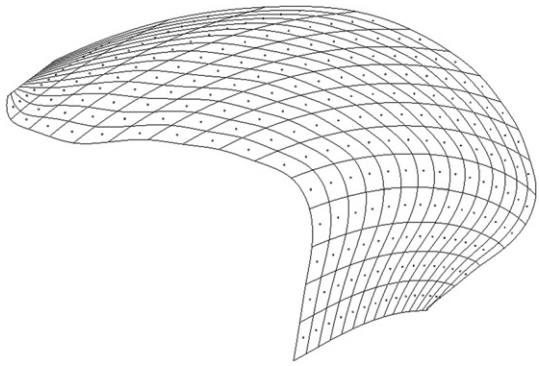

Fig. 4. Mesh of hydrodynamic sub-model (seen from the pressure side). The centroids of the elements are the control points where the pressure is evaluated. The corner points of the elements are the section points which define the geometry of the blade and are updated at each iteration step.

2) The hydrodynamic model mesh is updated based on the displacement field determined in the previous step. The updated position of the section points in the hydrodynamic model is that of the closest node in the structural model.
3) A new pressure field is determined by the hydrodynamic model based on the new shape.
4) The new pressure field given in the hydrodynamic model mesh is mapped onto the structural model. The new pressure value at each node of the structural model is determined by three-dimensional linear interpolation of the pressure calculated at the control points of the hydrodynamic model.

The process is repeated until convergence is achieved and equilibrium is found. The thrust and torque forces are calculated at each iteration. The iteration procedure has converged when the

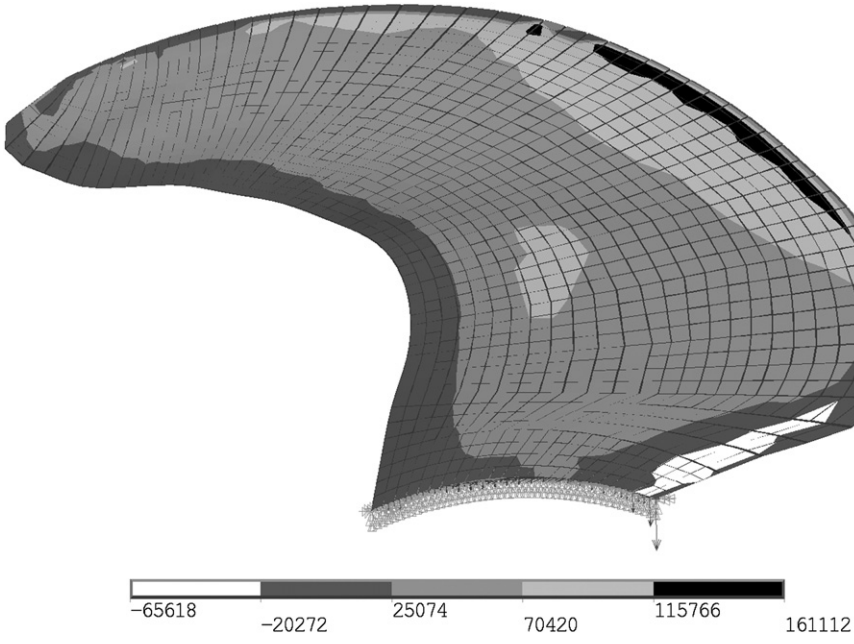

Fig. 5. Distribution of pressure difference (in Pa) over the blade surface looking in the upstream direction.

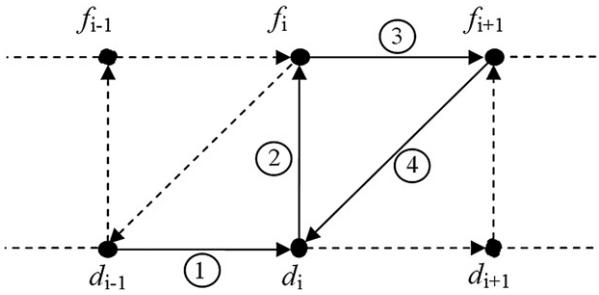

Fig. 6. Algorithm for the computation of the hydro-elastic steady state.

relative difference between the iterations of both thrust and torque is less than 1%. A typical convergence behaviour of the iteration procedure is presented in Fig. 7. According to the convergence criterion stated above, convergence is attained at the third iteration since the relative difference is below 1%. For illustrative purposes, the first 7 iterations are presented for the case where the convergence criterion has been switched off. In general the iterative procedure will converge after 3 or 4 iterations.

3.4. Optimization model

The maximum and cruising speed requirements for the ship and hence the thrust the propeller must generate are typically defined in the initial stage of the design process. Thus, the optimal propeller is the one which produces the desired thrust, the least torque, withstands the pressure forces, reduces the risk of cavitation and satisfies noise and vibration constraints. In this investigation the cavitation, noise and vibration constraints have been neglected. The strength constraints have not been included in the optimization model, but have instead been studied separately in parallel. The optimization problem is therefore posed as a torque minimization problem and formally stated as:

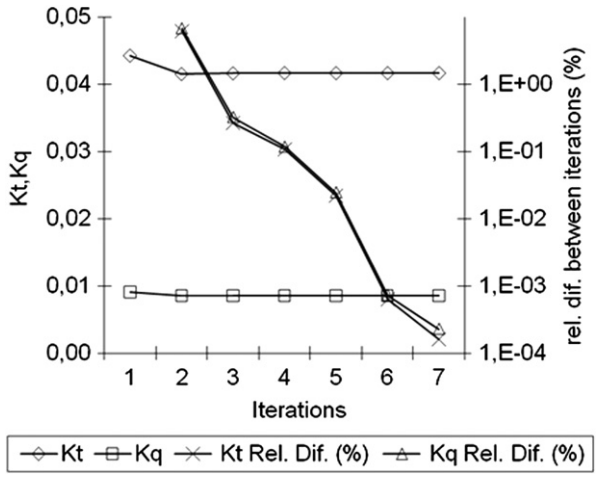

Fig. 7. Convergence behavior of the hydro-elastic model.

$$\min_{\theta_n \in \Re,\ \varphi_C \in \Re,\ \varphi_M \in \Re} CFOC(Q_C(\theta,\varphi_C), Q_M(\theta,\varphi_M)) \tag{2}$$

$$\begin{aligned} \textit{subject to}: & \frac{T_C^o(\theta,\varphi_C)}{T_C(\theta,\varphi_C)} - 1 \le 0 \\ & \frac{T_M^o(\theta,\varphi_M)}{T_M(\theta,\varphi_C)} - 1 \le 0 \\ & 0 \le \theta_n < 180 \\ & \varphi_{C,min} \le \varphi_C < \varphi_{C,max} \end{aligned}$$

where the combined fuel oil consumption, CFOC, is function of the torque at both conditions and is given by

$$CFOC(Q_C(\theta,\varphi_C), Q_M(\theta,\varphi_M)) = \Delta t_C \cdot SFOC_C \cdot 2\cdot\pi\cdot n_C \cdot Q_C(\theta,\varphi_C) + \Delta t_M \cdot SFOC_M \cdot 2\cdot\pi\cdot n_M \cdot Q_M(\theta,\varphi_M) \tag{3}$$

In the expressions above, the subscript *C*, *M* and *O* indicate *cruising*, *maximum* and *original* (or required), respectively. The CFOC is the weighted average of the fuel consumptions at the two operational conditions where the torque correspond to Q_C and Q_M, Δt is the percentage of time the ship operates at each of the forward speed conditions, *SFOC* is the specific fuel oil consumption and *n* is the propeller rotational speed. In this case it is assumed that the ship operates 90% of the time at cruising speed and 10% at maximum speed, i.e., $\Delta t_C = 0.9$ and $\Delta t_M = 0.1$. The specific fuel consumptions for each of the operation conditions are estimated to be $SFOC_C = 0.190$ kg/kWh and $SFOC_M = 0.540$ kg/kWh.

The design variables are the ply angles, θ, and the blade pitch angles φ_C and φ_M, all of which are assumed to vary continuously. The ply angles have been defined using two different approaches. In a first approach – *straight fiber path* approach – the ply angles are used directly as the design variables. A second approach – *curved fiber path* approach – uses a parameterization of θ inspired by the results of Parnas et al. [11]. The curved fiber paths represent a simple way to vary the properties of the laminate throughout the structure without increasing the number of design variables significantly. Thus the ply angles are defined as a function of a curved fiber path and the design variables become the parameters defining this path. The determination of the angle is as illustrated in Fig. 8. The ply angle at an element in position A or at any position with the same *z* coordinate is equal to the angle θ_e. This angle is determined by the tangent to the curve of a second degree polynomial defined by the points $c_0(y_0,z_0)$, $c_1(y_1,z_1)$ and $c_2(y_2,z_2)$. The design variables then become the parameters y_1 and y_2. The point c_0 and the coordinates z_1 and z_2 are assumed fixed.

The blade pitch angles, φ_C and φ_M, of the controllable pitch propeller are also included as design variables and can be adjusted independently for each operational condition. A change in the blade pitch angle corresponds to a rotation of the blade around the hub and consequently to a variation in the

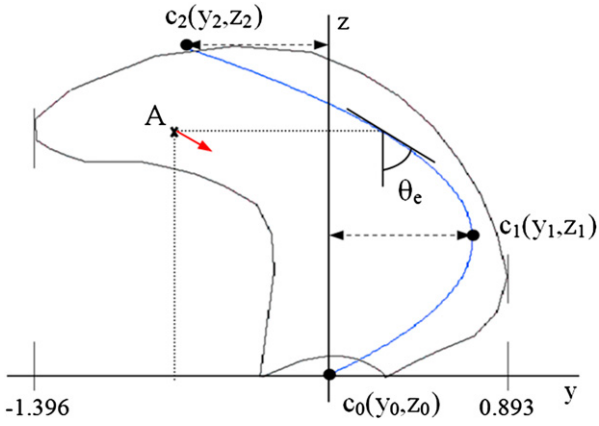

Fig. 8. Definition of the second degree curved fiber path.

angle of attack of all sections of the blade. In general, an increase in the blade pitch angle will correspond to an increase in the angle of attack of all sections and therefore to a variation in the lift and drag forces, and finally to an increase in the thrust and torque.

The constraints on the thrust, T_C and T_M, are included to assure that the optimal composite propeller will produce the same thrust as the original propeller. Note that the thrust is constrained from below indicating that the thrust may not be lower than the target thrust values. The inequality constraints are used (instead of equality constraints) due to the fact that the torque and thrust are coupled in their variations. That is, a decrease (or increase) in the torque will be accompanied by a decrease (or increase) in the thrust. Thus, the optimization model is limited by the thrust values as it tries to minimize the torque.

The choice of the optimization method depends heavily on the characteristics of the problem at hand. In this case the decision to opt for a gradient free method (as opposed to a gradient based method) is motivated by the low accuracy of the iterative method implemented for the determination of the hydro-elastic response. The gradient of the objective function and constraints cannot be defined analytically and therefore the alternative would be to resort to finite differences. The effect of the perturbations in the design variables is however not possible to measure as it cannot be distinguished from the oscillations resulting from the equilibrium iterations. The determination of the gradients is consequently compromised. The optimization model NOMADm [12] is therefore chosen. This is a type of derivative free, pattern-search algorithm specially suited for the analysis of nonlinear optimization problems where the gradients of the objective function and constraints are not available. Furthermore, NOMADm is combined with DACE [13] to form a surrogate model using spline interpolation which approximates the objective function and constraints. This procedure allows for a considerable reduction in the solution time of the optimization model.

4. Failure criteria

The strength of the blade is analyzed using a two dimensional version of the Tsai-Wu strength index (TWSI) [14] as given in Eq. (4),

$$TWSI = A + B \tag{4}$$

$$A = -\frac{\sigma_x^2}{\sigma_{x_t}^f \sigma_{x_c}^f} - \frac{\sigma_y^2}{\sigma_{y_t}^f \sigma_{y_c}^f} - \frac{\sigma_{xy}^f}{\left(\sigma_{xy}^f\right)^2} \frac{C_{xy}\sigma_x\sigma_y}{\sqrt{\sigma_{x_t}^f \sigma_{x_c}^f \sigma_{y_t}^f \sigma_{y_c}^f}}$$

$$B = \left(\frac{1}{\sigma_{x_t}^f} + \frac{1}{\sigma_{x_c}^f}\right)\sigma_x + \left(\frac{1}{\sigma_{y_t}^f} + \frac{1}{\sigma_{y_c}^f}\right)\sigma_y$$

where C_{xy} is an empirical parameter typically assumed as 0.5. The remaining terms are described together with Table 3. The TWSI is a quadratic multiaxial failure criterion specially developed for orthotropic materials where an index above one indicates material failure.

$$\begin{aligned}
&\textit{fiber tension} : \frac{\sigma_x}{\sigma_{x_t}^f} \quad \textit{if} \quad \sigma_x > 0 \\
&\textit{Matrix tension} : \frac{\sigma_y}{\sigma_{y_t}^f} \quad \textit{if} \quad \sigma_y > 0 \\
&\textit{Matrix tension} : \frac{\sigma_y}{\sigma_{y_t}^f} \quad \textit{if} \quad \sigma_y > 0 \\
&\textit{Fiber compression} : \frac{\sigma_x}{\sigma_{x_c}^f} \quad \textit{if} \quad \sigma_x > 0 \\
&\textit{Matrix compression} : \frac{\sigma_y}{\sigma_{y_c}^f} \quad \textit{if} \quad \sigma_y > 0 \\
&\textit{In-plane shear} : \frac{\sigma_{xy}}{\sigma_{xy}^f}
\end{aligned} \tag{5}$$

The main disadvantage of the TWSI is that it is not possible to distinguish between the contributions of the different failure modes. In order to overcome this limitation, the Maximum Stress Failure Criterion (MSFC) is used in parallel with the TWSI. The stress ratios in Eq. (5) have been determined at

each layer of all elements. The critical failure mode will then be the mode with largest associated ratio over all layers. It is possible in this way to determine the dominating failure mode at each element in the blade.

5. Results

In the following, notice that the optimization and strength analysis steps are performed in parallel. The laminate properties are optimized first. The strength of the blade is subsequently analyzed and the necessary reinforcements are included on a trial and error basis. The laminate properties are then once again optimized but this time the properties of the laminate in the critically stressed regions are kept fixed. All results are obtained using the shell element model. The ply angle reference axes as well as the blade coordinate system are presented in Fig. 9. The *x* axis points in the upstream direction (direction of forward motion of the ship). The propeller rotates in the clockwise direction when looking upstream.

5.1. Effect of fiber orientation on blade properties

Before proceeding with the optimization of the laminate lay-up, several simple tests were conducted to investigate the influence of the fiber orientation on the propulsive and geometrical properties of the blade. Initially the analysis is conducted assuming that the blade consists of one laminate with one single lamina angle, i.e., $[(\theta)_{32}]$ over the entire blade. The variations in the fuel consumption, thrust and torque are then calculated as functions of the ply angle, θ, for both cruising and maximum speed operation conditions. The results are presented in Fig. 10 and are defined as ratios between the calculated values from the composite blade and those of the original blade. The case where the thrust

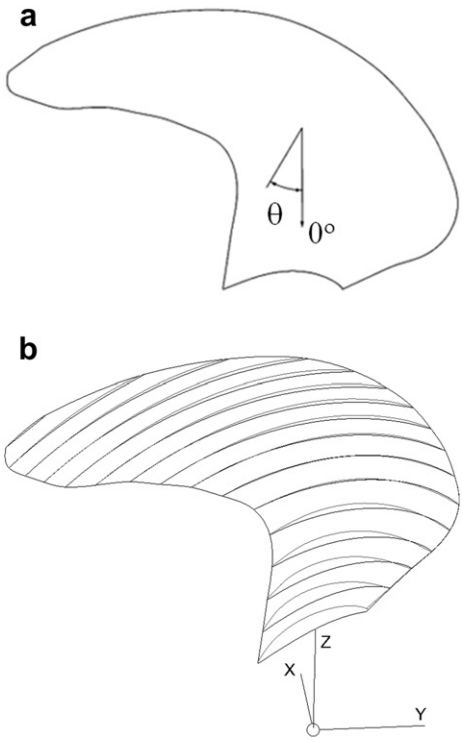

Fig. 9. (a) Ply angle orientation reference axis. (b) Blade coordinate system: *x*-direction corresponds to the forward speed direction, *y*-direction points in the starboard direction of the ship and the *z*-direction is the vertical direction of the blade. The *yz*-plane coincides with the plane of rotation of the propeller.

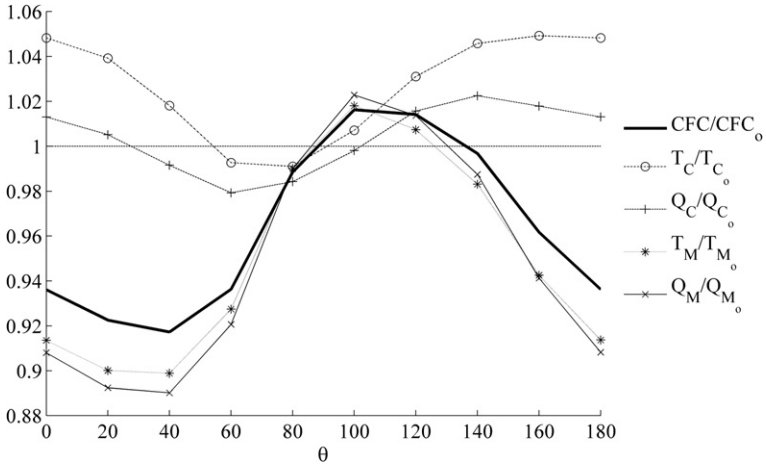

Fig. 10. Combined fuel consumption (CFOC), thrust (T) and torque (Q) ratios between the composite and original blade for varying lamina angle, given for both the cruising and maximum speed conditions.

or torque ratio is above one indicates fiber angles for which the composite propeller generates more thrust or torque than the original one. The same holds for the fuel consumption. Furthermore, if the thrust ratio is larger than the torque ratio then the efficiency of the composite propeller is higher than the original. Thus, in the cruising speed condition the efficiency of the composite blade is higher than the original for any fiber orientation since the thrust ratio is always higher than the torque ratio. The thrust generated by the composite propeller only matches that of the original blade when the fiber angle is around 50° and 90°. In the maximum speed condition the efficiency of the composite propeller is lower than the original for ply angles between 80° and 150°, and higher otherwise. Concerning the generated thrust, in this case it only matches the target values for fiber angles close to 80° and 130°.

As mentioned before, the optimal composite propeller minimizes the fuel consumption or torque while generating the same thrust force as the original. Hence, the aim is to find one fiber orientation for which the thrust ratio is equal to one (i.e., equal to the required) and the torque ratio is lower than unity (or lower than the original) for both operating conditions simultaneously. This case is not verified for any of the fiber angles presented in Fig. 10. The inclusion of the blade pitch angles as design variables in the optimization model is consequently justified. By varying the blade pitch angles for each operation condition independently it is possible to compensate for any necessary variations of the thrust and torque.

All the parameters describing the blade geometry presented in Table 1 were analyzed for the two ply angles where thrust and torque reach their maximum and minimum values. From Fig. 10 it is possible to see that the respective ply angles are 80° (minimum value) and 160° (maximum value) for the cruising speed condition and 40° (minimum value) and 100° (maximum value) for the maximum speed condition. The largest variations were observed in the radial distributions of pitch, camber and mid-chord positions (see Fig. 11). The radial distribution of pitch tends to be equal or lower than the original rigid blade (see Fig. 11(a,b)), whereas the camber tends to be larger in sections close to the hub and lower close to the tip (see Fig. 11(c,d)). The only exception being the maximum speed case for $[(100^\circ)_{32}]$ where the camber of most sections is larger than for the original blade. As expected for both cases the blade has deformed in the upstream direction (see Fig. 11(e,h)). At maximum speed the effect of the fiber direction on the local stiffness of the tip region is visible (see Fig. 11(f)). A laminate lay-up of $[(100^\circ)_{32}]$ will reinforce the tip whereas a laminate $[(40^\circ)_{32}]$ will result in more local flexibility.

Generally an increase in pitch and camber will correspond to an increase in the lift force (assuming there is no flow separation) and consequently also in the thrust and torque. Based on the results from Fig. 11 it is however difficult to establish the relation between the variation of the propulsive forces and the geometrical characteristics of the composite blade.

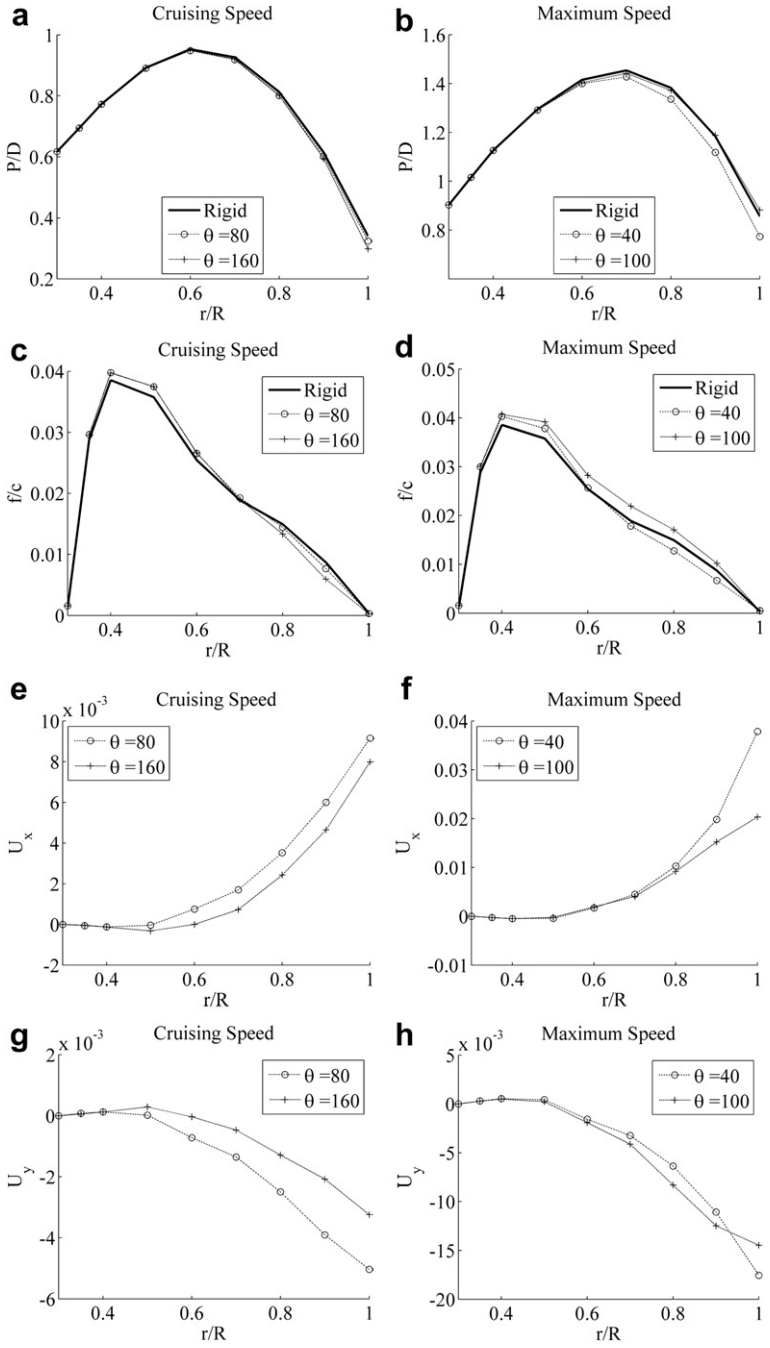

Fig. 11. Radial distributions of pitch (a,b), camber (c,d), displacement in *x*-direction (cf. Fig. 9(b)) of mid-chord point (e,f) and displacement in *y*-direction (cf. Fig. 9(b)) of mid-chord point (g,h). Results for the cruising speed condition are for laminate lay-ups $[(80^\circ{}_{32})]$ and $[(160^\circ)_{32}]$, and $[(40^\circ)_{32}]$ and $[(100^\circ)_{32}]$ for the maximum speed condition.

5.2. Optimization of laminate lay-up

The first optimization results are obtained using the straight fiber path approach where the following three laminate configurations are tested: $[(\theta_1)_{32}]$, $[(\theta_1)_8, (\theta_2)_8, (\theta_3)_8, (\theta_4)_8]$ and $[(\theta_1)_8, (\theta_2)_8]_s$. The optimal fiber angles, resulting fuel consumption reduction and optimal blade pitch angles for all three laminate configurations are presented in Table 4. All laminate configurations converge to approximately the same lay-up – $[(40^\circ)_{32}]$ – and the one layer case is that which holds the largest reduction in fuel consumption. The fiber angles for this case are presented in Fig. 12 (a).

At maximum speed the thrust and torque are exactly equal to that of the original blade. Nonetheless, a reduction of 4.2% in the fuel consumption was found at the cruising speed condition corresponding to 1.12% in the combined case. The latter results suggest that the variation of the ply angles through the thickness has little influence on the blade response. This is in agreement with the presumption that the coupling effects are maximized for a laminate whose layers are mostly oriented in the same direction. This is also a direct consequence of the fact that the optimization model searches only for the optimal stiffness distribution and neglects other effects like stress constraints.

In the next step, the laminate angles are defined using the curved fiber path approach described earlier. The following laminate configurations are used in the analysis: $[(\theta_1(y_1,y_2))_{32}]$, $[(\theta_1(y_1^1,y_2^1))_{16}, (\theta_2(y_1^2,y_2^2))_{16}]$ and $[(\theta_1(y_1^1,y_2^1))_8, (\theta_2(y_1^2,y_2^2))_8, (\theta_3(y_1^3,y_2^3))_8, (\theta_4(y_1^4,y_2^4))_8]$. The results of the optimization analysis showed once again that the blade performance is not sensitive to the variations of the angles through the thickness. The optimal laminate lay-up $[(\theta_1(0.756,0.677))_{32}]$ is therefore chosen as illustrated in Fig. 12(b). The resulting decrease in the fuel consumption amounted to 4.7% at cruising speed corresponding to a reduction of 1.25% in the combined case (see Table 4). This corresponds to a further decrease of 0.13% in the combined fuel consumption when compared to the straight fiber path approach.

Finally, it should be noted that all optimal laminate configurations promote a flexible tip (cf. Fig. 11(f)). In the curved fiber path case, the maximum displacement occurs at the tip and is approximately 50 mm. Furthermore, the weight of the composite blade is approximately 230 kg, or around 1/4 of the weight of the original metal blade which is 1087 kg (assuming $\rho_{metal} \approx 7800\ kg/m^3$).

5.3. Strength analysis

All results presented hereafter are obtained for the maximum speed condition since this was identified as the most critical load condition of the two considered in this investigation. However, the backing and crash-stop conditions have been neglected in this investigation. The maximum TWSI over all layers at each element is plotted in Fig. 13(a). The maximum TWSI targeted during the design process is 0.7 since this is considered to be a reasonable level of safety in a practical design situation. The strength analysis is performed in parallel with the optimization of the fiber angles. The optimal

Table 4
Optimal laminate configurations and blade pitch angles (P/D_{07}). The thrust ration for the cruising and maximum speed conditions are given by (T_C/T_{C0}) and (T_M/T_{M0}), respectively. The percentage reduction in fuel consumption is given by ($\%FC_S$).

Laminate		Cruising Speed			Maximum Speed			Combined
		P/D_{07}	T_C/T_{C0}	$\%FC_S$	P/D_{07}	T_M/T_{M0}	$\%FC_S$	$\%FC_S$
$[(\theta_1)_{32}]$	$[(40^\circ)_{32}]$	0.544	1.00	4.2	2.412	1.00	0.0	1.12
$[(\theta_1)_8, (\theta_2)_8, (\theta_3)_8, (\theta_4)_8]$	$[(40.2^\circ)_8, (40.2^\circ)_8, (30.7^\circ)_8, (39.3^\circ)_8]$	0.611	1.00	3.5	2.391	1.00	0.0	0.94
$[(\theta_1)_8, (\theta_2)_8]_s$	$[(41.8^\circ)_8, (42.4^\circ)_8]_s$	0.635	1.00	3.3	2.372	1.00	0.0	0.89
$[(\theta_1(y_1^1,y_2^1))_{32}]$	$[(\theta_1(0.756,0.677))_{32}]$	0.512	1.00	4.7	2.550	1.00	0.0	1.25
$[(\theta_1(y_1^1,y_2^1))_{16}, (\theta_2(y_1^2,y_2^2))_{16}]$	$[(\theta_1(0.767,0.694))_{16}, (\theta_2(0.764,0.689))_{16}]$	0.514	1.00	4.7	2.467	1.00	0.0	1.25
$[(\theta_1(y_1^1,y_2^1))_8, (\theta_2(y_1^2,y_2^2))_8, (\theta_3(y_1^3,y_2^3))_8, (\theta_4(y_1^4,y_2^4))_8]$	$[(\theta_1(0.765,0.694))_8, (\theta_2(0.757,0.678))_8, (\theta_3(0.759,0.680))_8, (\theta_4(0.767,0.693))_8]$	0.514	1.00	4.7	2.464	1.00	0.0	1.25

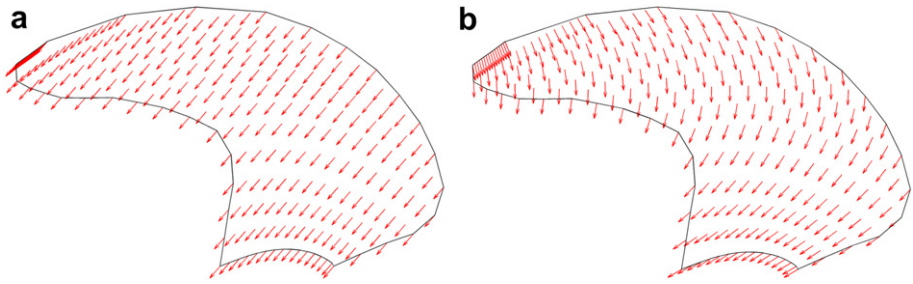

Fig. 12. (a) Resulting fiber angles obtained using straight fiber paths. (b) Resulting fiber angles obtained using curved fiber paths.

fiber angles are defined first and the strength of the resulting lay-up is examined next. The critical regions where the TWSI reaches the highest value are identified as the trailing edge and hub regions. The lay-up at these regions is then modified on a trial and error basis in order to reduce the maximum TWSI. The following lay-up sequences were consequently found: regions 1, 2, 3 and 4 (cf. Fig. 13(a)) are respectively changed to $[(-45^\circ)_{32}]$, $[(0^\circ)_{32}]$, $[(0^\circ)_{32}]$ and $[(90^\circ)_{32}]$.Finally, the lay-up of the critical regions is fixed while the optimal fiber angles in the remaining parts of the blade is optimized once again. Notice that the results from Table 4 refer to this final case where the laminate of the critical regions has been fixed and the remaining laminate over the entire blade has been optimized a second time.

Finally, the failure modes which according to the MSFC (Eq. (5)) show the largest ratios at each element are presented in Fig. 13(b). The results indicate that the laminates in the leading and trailing edge regions close to the hub, and in the central part of the blade close to the tip, may fail due to in-plane shear and matrix compression. The effect of the reinforcements is particularly visible in the trailing edge region. Before the re-orientation of the fibers in those regions was adopted, matrix failure was the failure mode with the largest ration whereas after the re-orientation of the fibers, in-plane shear is the failure mode holding the largest ration.

6. Discussion

Overall the results indicate that it is possible to tailor the orthotropic properties of laminated composite materials to design a flexible composite propeller whose shape passively adapts to the different working conditions while resisting the imposed loads. Optimal fiber orientations have been identified which result in a decrease of the fuel consumption. It is important to note though that the hydrodynamic model does not account for flow separation or cavitation. Consequently the resulting

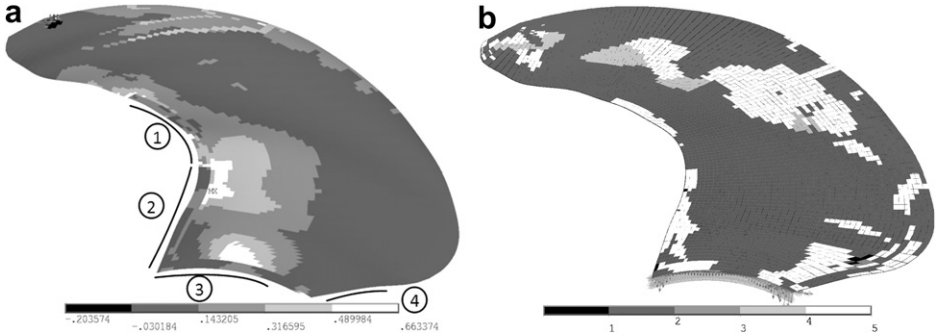

Fig. 13. (a) Maximum TWSI over all layers for the optimal propeller blade with curved fiber path. The regions 1, 2, 3 and 4 indicate regions with the lay-up configurations: $[(-45^\circ)_{32}]$, $[(0^\circ)_{32}]$, $[(0^\circ)_{32}]$ and $[(90^\circ)_{32}]$. (b) Failure modes for layer with highest stress ratios (see Eq. (5)) for each element. Legend: (1) – Fiber tension; (2) – Matrix tension; (3) – Fiber compression; (4) – Matrix compression; (5) – In-plane shear stress.

optimal blade pitch angles may be too large. Furthermore, the results indicate a possibility for reducing the fuel consumption further by varying the laminate orientation across the length and width of the blade, e.g., using curved fiber paths. However, these variations in the fiber alignment may be difficult to achieve in practice in which case the straight fiber path results should be used as reference.

From a strength point of view, the TWSI has been used to identify overly stressed blade areas while the MSFC provided information as to the failure modes with the highest possibility of failure. The laminate in the critical regions was consequently redesigned and the TWSI was decreased. The proposed laminate orientations however disregard once again production constraints and would need to be revised in a subsequent iteration of the design process. In this sense, the analysis model used in this investigation assumes that all layers have the same thickness. An analysis model incorporating ply drop-off to account for changes in thickness should also be considered at a later stage for a more accurate evaluation of the strength properties. Besides, the full reverse and crash-stop conditions should be considered as well since these are usually critical load cases. Finally, propeller blades are subjected to cyclic loads and the analysis of the effects due to fatigue is therefore strongly recommended.

7. Conclusions

A framework for the design and optimization of composite marine propellers has been presented. The laminate lay-up configuration and blade pitch angles of a large naval type controllable pitch composite propeller blade with high skew was optimized for two different load conditions – cruising and maximum speed. Two parameterizations of the fiber angles have been considered in the optimization model. Namely, the straight fiber path approach which assumes constant fiber angles throughout the blade and the curved fiber path approach which assumes that the orientation of the fibers throughout the blade follows a polynomial curve. The largest reduction in fuel consumption was obtained using the curved fiber path approach. The optimal fiber and blade pitch angles have been determined and a reduction of the combined fuel consumption of 1.25%, corresponding to a decrease of 4.7% for the cruising speed and no reduction for the maximum speed condition, was observed.

Concerning the geometrical properties of the blade, the largest variations were observed in the radial distributions of pitch, camber and mid-chord positions. The optimal configurations promoted a flexible tip and a stiff body closer to the hub.

The strength of the blade was analysed in terms of the Tsai-Wu strength index and performed in parallel with the optimization of the fiber and blade pitch angles. The leading edge and hub regions were identified as the critical areas. The blade was therefore reinforced and the lay-up configuration in these regions was modified. It was shown that after reinforcement of the critical areas, the maximum Tsai-Wu failure index was lowered from 1.6 to around 0.7 suggesting that no failure occurs. The most significant failure modes were identified as matrix failure in tension and in-plane shear.

The results are encouraging and suggest that it should be possible to build a large flexible composite marine propeller which outperforms its metal counterpart.

Acknowledgements

This work has been performed within the Network of Excellence on Marine Structures (MARSTRUCT) and has been partially funded by the European Union through the Growth Programme under contract TNE3-CT-2003-506141.

The invaluable support given by Associate Professor Mathias Stolpe, Department of Mathematics, Technical University of Denmark is gratefully acknowledged.

References

[1] Berring P, Branner K, Berggreen C, Knudsen HW, "Torsional performance of wind turbine blades – Part I: Experimental investigation", 16th International Conference on Composite Materials (ICCM-16), Kyoto, Japan, July 8–13, 2007.

[2] Branner K, Berring P, Berggreen C, Knudsen HW, "Torsional performance of wind turbine blades – Part II: Numerical verification", 16th International Conference on Composite Materials (ICCM-16), Kyoto, Japan, July 8–13, 2007.

[3] Lobitz DW, Veers PS, Eisler GR, Laino DJ, Migliore PG, Bir G. The use of twist coupled blades to enhance the performance of horizontal axis wind turbines. SANDIA Report SAND2001–1303.
[4] Livne E, Weisshaar TA. Aeroelasticity of non-conventional airplane configurations-past and future. Journal of Aircraft 2003;40(6):1047–65.
[5] Ganguli R, Chopra I. Aeroelastic optimization of a helicopter rotor with composite coupling. Journal of Aircraft 1995;32(6): 1326–34.
[6] Lee YJ, Lin CC. Optimized design of composite propellers. Mechanics of Advanced Materials and Structures 2004;11:17–30.
[7] Lin HJ, Lin JJ, Chuang TJ. Strength evaluation of a composite marine propeller blade. Journal of Reinforced Plastics and Composites 2004;24(17):1791–807.
[8] Marsh G. A new start for marine propellers? Reinforced Plastics, December, 2004.
[9] Zenkert D, Battley M. Foundations of fiber composites. Royal Institute of Technology, Paper 96–10.
[10] www.ansys.com.
[11] Parnas L, Oral S, Ceyhan Ü. Optimum design of composite structures with curved fiber paths. Composites Science and Technology 2003;63:1071–82.
[12] Booker AJ, Dennis JE, Frank PD, Serafini DB, Torczon V, Trosset MW. A rigorous framework for the optimization of expensive functions by surrogates. Technical Report CRPC-TR98739-S, Center for Research on Parallel Computation, Rice University; 1998.
[13] Lophaven SN, Nielsen HB, Søndergaard J. DACE – A MATLAB Kriging Toolbox. Technical Report IMM-TR-2002–12.
[14] Tsai SW, Wu EM. A general theory of strength for anisotropic materials. Journal of Composite Materials 1971;5:58–80.